

Error Bounds for Variational Quantum Time Evolution

Christa Zoufal,^{1,2} David Sutter,¹ and Stefan Woerner¹

¹*IBM Quantum, IBM Research – Zurich*

²*Institute for Theoretical Physics, ETH Zurich*

Variational quantum time evolution (VarQTE) allows us to simulate dynamical quantum systems with parameterized quantum circuits. We derive a posteriori, global phase-agnostic error bounds for real and imaginary time evolution based on McLachlan’s variational principle that can be evaluated efficiently. Rigorous error bounds are crucial in practice to adaptively choose variational circuits and to analyze the quality of optimization algorithms. The power of the new error bounds, as well as, the performance of VarQTE are demonstrated on numerical examples.

I. INTRODUCTION

In 1981, Richard Feynman suggested the development of quantum computers with the following words, "Nature isn't classical, dammit, and if you want to make a simulation of nature, you'd better make it quantum mechanical, and by golly it's a wonderful problem, because it doesn't look so easy." In many cases the simulation of a quantum mechanical nature corresponds to *quantum time evolution* (QTE). Applications of QTE are numerous and range from simulating Ising models [1], to approximating quantum Gibbs states [2–6], to solving combinatorial optimization problems [7]. In order to implement QTE on a gate-based quantum computer, the respective evolution needs to be translated into quantum gates. This translation can, e.g. be approximated with Trotterization [3, 8]. Depending on the evolution time and expected accuracy, this approach may lead to deep quantum circuits and is, thus, not well-suited for near-term quantum computers.

Variational quantum time evolution (VarQTE) [9, 10] is a powerful and versatile approach to simulate quantum time dynamics with parameterized quantum circuits. Due to its compatibility with shallow, parameterized circuits, VarQTE displays a promising approach to utilize near-term devices for solving practically relevant tasks. The usage of short circuits results in a limited expressivity of the available parameterized unitaries and implies that VarQTE generally comes with an approximation error. It is crucial to quantify this error, to be able to interpret the results, and to possibly rerun simulations with more expressive parameterized circuits in case the error is too large.

In this work, we derive new a posteriori error bounds for variational quantum real and imaginary time evolution which we shall refer to as VarQRTE and VarQITE, respectively. The obtained error bounds allow us to efficiently, quantify the approximation error with respect to the optimal QTE. The bounds are phrased in terms of the Bures metric and are, hence, agnostic to physically irrelevant global phase mismatches – a feature that is crucial for practical applications. This represents an improvement compared to existing results [11]. Thus, they directly define lower bounds on the fidelity between prepared and target states. The power of the novel error bounds is demonstrated on various numerical examples.

We, thereby, also investigate their performance and illustrate the application to concrete settings.

The structure of this work is as follows. First, we explain the concepts of (variational) quantum time evolution in Sec. II. Then, Sec. III introduces the a posteriori error bounds for VarQRTE and VarQITE. Furthermore, methods used for the numerical experiments are described in Sec. IV and the respective results are presented in Sec. V. Finally, conclusions and outlook are given in Sec. VI.

II. VARIATIONAL QUANTUM TIME EVOLUTION

QTE describes the process of evolving a quantum state over time with respect to a Hamiltonian H . Real time evolution enables the study of unitary quantum dynamics described by $e^{-iHt/\hbar}$ for $t \in \mathbb{R}$, e.g., of fermionic models such as the Hubbard model [12]. If the time parameter t is replaced by an imaginary time it the system dynamics change to a non-unitary evolution. Suppose that the initial state has a non-zero overlap with the ground state of H , then all components that do not correspond to the ground state are damped exponentially in time during imaginary time evolution. This form of time evolution is, thus, a particularly useful tool to find the ground state of H [9]. Furthermore, imaginary time evolution can be used to solve partial differential equations [13–15] or to prepare quantum Gibbs states [2, 10]. A generalized time evolution can be used to do matrix multiplications, solve systems of linear equations and combine real and imaginary time evolution [16].

VarQTE approximates the target state $|\psi_t^*\rangle$ with a state $|\psi_t^\omega\rangle$ whose time dependence is projected onto the parameters ω_t of a variational ansatz. To simplify the notation, the time parameter t is dropped from $\omega = (\omega_0, \dots, \omega_k) \in \mathbb{R}^{k+1}$ in the remainder of this work when referring to the ansatz parameters. More specifically, we consider a formulation for pure states based on McLachlan’s variational principle [17] with a global phase agnostic evolution [10]. The state evolution described by this variational principle corresponds to an initial value problem where the underlying *ordinary differential equation* (ODE) [18] is derived from McLachlan’s variational prin-

ciple [17]. We simulate the time evolution by numerically solving the ODE for a set of initial parameter values.

In the following, real and imaginary time evolution, as well as, the variational implementations are introduced. The respective notation is simplified by setting $\hbar = 1$.

A. Variational Quantum Real Time Evolution

The time-dependent Schrödinger equation describes the change of a state $|\psi_t^*\rangle$ under real time evolution

$$i |\dot{\psi}_t^*\rangle = H |\psi_t^*\rangle, \quad (1)$$

where we write the time derivative as $|\dot{\psi}_t^*\rangle = \frac{\partial |\psi_t^*\rangle}{\partial t}$. The resulting time-dependence of the state reads

$$|\psi_t^*\rangle = e^{-iHt} |\psi_0^*\rangle. \quad (2)$$

Next, the variational implementation for the real time evolution of a parameterized state $|\psi_t^\omega\rangle$ is discussed. To that end, we employ a VarQTE approach which is agnostic to a potential time-dependent global phase [10]. The respective variational principle is derived in the following.

Consider the real time evolution of a parameterized state with an explicit time-dependent global phase parameter ν , i.e., $|\psi_t^\nu\rangle = e^{-i\nu} |\psi_t^\omega\rangle$ for $\nu = \nu_t \in \mathbb{R}$, where

$$|\dot{\psi}^\nu\rangle = -i\dot{\nu} e^{-i\nu} |\psi_t^\omega\rangle + e^{-i\nu} |\dot{\psi}_t^\omega\rangle. \quad (3)$$

The Schrödinger equation with respect to $|\psi_t^\nu\rangle$ reads

$$i |\dot{\psi}^\nu\rangle = H |\psi^\nu\rangle \quad (4)$$

and can be rewritten as

$$i e^{-i\nu} |\dot{\psi}_t^\omega\rangle = (H - i\dot{\nu}) e^{-i\nu} |\psi_t^\omega\rangle. \quad (5)$$

To simplify the notation, we shall from now on refer to $i\dot{\nu}$ as $\dot{\nu}$. Division by $e^{-i\nu}$ gives

$$i |\dot{\psi}_t^\omega\rangle = (H - \dot{\nu}) |\psi_t^\omega\rangle. \quad (6)$$

Applying McLachlan's variational principle [17] to Eq. (6) leads to

$$\delta \left\| i |\dot{\psi}_t^\omega\rangle - (H - \dot{\nu}) |\psi_t^\omega\rangle \right\|_2 = 0, \quad (7)$$

where $\|x\|_2 = \sqrt{\langle x, x \rangle}$. To find an explicit expression for $\dot{\nu}$, we evaluate the respective variational principle, i.e.,

$$\delta_{\dot{\nu}} \left\| i |\dot{\psi}_t^\omega\rangle - (H - \dot{\nu}) |\psi_t^\omega\rangle \right\|_2 = 0 \quad (8)$$

which leads to

$$\dot{\nu} = E_t^\omega + \text{Im} \left(\langle \dot{\psi}_t^\omega | \psi_t^\omega \rangle \right), \quad (9)$$

where $E_t^\omega := \langle \psi_t^\omega | H | \psi_t^\omega \rangle$.

Finally, we can see that Eq. (5) defines an evolution for $|\psi_t^\omega\rangle$ that simulates the existence of the global phase parameter ν without actually integrating or tracking $e^{-i\nu}$, i.e.,

$$i |\dot{\psi}_t^\omega\rangle = H |\psi_t^\omega\rangle, \quad (10)$$

where $|\dot{\psi}_t^\omega\rangle := |\dot{\psi}_t^\omega\rangle - i(E_t^\omega + \text{Im}(\langle \dot{\psi}_t^\omega | \psi_t^\omega \rangle)) |\psi_t^\omega\rangle$ represents the effective state gradient. McLachlan's variational principle now implies

$$\delta \| i |\dot{\psi}_t^\omega\rangle - H |\psi_t^\omega\rangle \|_2 = 0. \quad (11)$$

Since $|\psi_t^\omega\rangle$ is given by a parameterized quantum circuit, solving Eq. (11) with $|\dot{\psi}_t^\omega\rangle = \sum_i \dot{\omega}_i \frac{\partial |\psi_t^\omega\rangle}{\partial \omega_i}$ results in [10]

$$\sum_{j=0}^k \mathcal{F}_{ij}^Q \dot{\omega}_j = \text{Im} \left(C_i - \frac{\partial \langle \psi_t^\omega |}{\partial \omega_i} |\psi_t^\omega\rangle E_t^\omega \right), \quad (12)$$

where $C_i = \frac{\partial \langle \psi_t^\omega |}{\partial \omega_i} H |\psi_t^\omega\rangle$ and \mathcal{F}_{ij}^Q denotes the (i, j) -entry of the Fubini-Study metric [19, 20] given by

$$\mathcal{F}_{ij}^Q = \text{Re} \left(\frac{\partial \langle \psi_t^\omega |}{\partial \omega_i} \frac{\partial |\psi_t^\omega\rangle}{\partial \omega_j} - \frac{\partial \langle \psi_t^\omega |}{\partial \omega_i} |\psi_t^\omega\rangle \langle \psi_t^\omega | \frac{\partial |\psi_t^\omega\rangle}{\partial \omega_j} \right).$$

We would like to point out that for pure states the Fubini-Study metric is proportional to the quantum Fisher Information matrix. The efficient evaluation of the terms in Eq. (12) is discussed in Appendix E.

Solving the system of linear equations (SLE) [21] from Eq. (12) for $\dot{\omega}$ defines an ODE that describes the evolution of the parameters, i.e.,

$$f_{\text{std}}(\omega) = (\mathcal{F}^Q)^{-1} \text{Im} \left(\mathbf{C} - \frac{\partial \langle \psi_t^\omega |}{\partial \omega} |\psi_t^\omega\rangle E_t^\omega \right), \quad (13)$$

with $\mathbf{C} = (C_0, \dots, C_k)$.

Notably, the gradient $|\dot{\psi}_t^\omega\rangle$ computed on the basis of this variational principle will not always be exact. Therefore, $\| |e_t\rangle \| > 0$ where

$$|e_t\rangle := |\dot{\psi}_t^\omega\rangle + iH |\psi_t^\omega\rangle \quad (14)$$

denotes the gradient error. This gradient error also enables an alternative definition of a VarQRTE ODE. More explicitly, we can define the ODE as optimization problem that searches for the minimizing argument of the squared gradient error norm,

$$f_{\text{min}}(\omega) = \underset{\omega \in \mathbb{R}^{k+1}}{\text{argmin}} \| |e_t\rangle \|_2^2, \quad (15)$$

which can also be written as

$$\begin{aligned} \| |e_t\rangle \|_2^2 &= \text{Var}(H)_{\psi_t^\omega} + \left(\langle \dot{\psi}_t^\omega | \dot{\psi}_t^\omega \rangle - \langle \dot{\psi}_t^\omega | \psi_t^\omega \rangle \langle \psi_t^\omega | \dot{\psi}_t^\omega \rangle \right) \\ &\quad - 2\text{Im} \left(\langle \dot{\psi}_t^\omega | H | \psi_t^\omega \rangle - E_t^\omega \langle \dot{\psi}_t^\omega | \psi_t^\omega \rangle \right), \end{aligned} \quad (16)$$

with $\text{Var}(H)_{\psi_t^\omega} = \langle \psi_t^\omega | H^2 | \psi_t^\omega \rangle - (E_t^\omega)^2$ and $2\text{Re}(\langle \psi_t^\omega | \dot{\psi}_t^\omega \rangle) = \frac{\partial \langle \psi_t^\omega | \psi_t^\omega \rangle}{\partial t} = 0$.

Since the time-dependence of $|\psi_t^\omega\rangle$ is encoded in the real parameters ω , Eq. (16) can, therefore, be rewritten as

$$\begin{aligned} \| |e_t\rangle \|_2^2 &= \text{Var}(H)_{\psi_t^\omega} + \sum_{i,j} \dot{\omega}_i \dot{\omega}_j \mathcal{F}_{ij}^Q \\ &\quad - 2 \sum_i \dot{\omega}_i \text{Im} \left(C_i - \frac{\partial \langle \psi_t^\omega |}{\partial \omega_i} | \psi_t^\omega \rangle E_t^\omega \right) \end{aligned} \quad (17)$$

using

$$\begin{aligned} &\text{Im} \left(\langle \dot{\psi}_t^\omega | H | \psi_t^\omega \rangle - E_t^\omega \langle \dot{\psi}_t^\omega | \psi_t^\omega \rangle \right) \\ &= \sum_i \dot{\omega}_i \text{Im} \left(C_i - \frac{\partial \langle \psi_t^\omega |}{\partial \omega_i} | \psi_t^\omega \rangle E_t^\omega \right) \end{aligned} \quad (18)$$

and

$$\langle \dot{\psi}_t^\omega | \psi_t^\omega \rangle - \langle \dot{\psi}_t^\omega | \psi_t^\omega \rangle \langle \psi_t^\omega | \dot{\psi}_t^\omega \rangle = \sum_{i,j} \dot{\omega}_i \dot{\omega}_j \mathcal{F}_{ij}^Q. \quad (19)$$

This reformulation enables the evaluation of the norm since the individual terms can be efficiently computed.

We would like to point out that solving Eq. (13) with a least square solver is analytically equivalent to solving Eq. (15). However, the simulation results in Sec. V show that the numerical behavior of the latter is more stable.

B. Variational Quantum Imaginary Time Evolution

Imaginary time evolution of a quantum state is mathematically described by the normalized, Wick-rotated Schrödinger equation

$$|\dot{\psi}_t^*\rangle = (E_t^* \mathbf{1} - H) |\psi_t^*\rangle, \quad (20)$$

where $E_t^* = \langle \psi_t^* | H | \psi_t^* \rangle$ corresponds to the system energy. In the remainder of this work, the notation for $E_t^* \mathbf{1} - H$ is simplified to $E_t^* - H$. The state evolution reads

$$|\psi_t^*\rangle = \frac{e^{-Ht} |\psi_0^*\rangle}{\sqrt{\langle \psi_0^* | e^{-2Ht} | \psi_0^* \rangle}}. \quad (21)$$

Analogously to Sec. II A, we use a VarQITE implementation for $|\psi_t^*\rangle$ that simulates the existence of an explicit global phase $e^{-i\nu}$ [9, 10]. The normalized, Wick-rotated Schrödinger equation of an evolution of the state $|\psi_t^\nu\rangle = e^{-i\nu} |\psi_t^*\rangle$ reads

$$|\dot{\psi}^\nu\rangle = (E_t^\omega - H) |\psi^\nu\rangle, \quad (22)$$

where

$$|\psi^\nu\rangle = e^{-i\nu} |\psi_t^\omega\rangle - i\nu e^{-i\nu} |\psi_t^\omega\rangle. \quad (23)$$

Thus,

$$e^{-i\nu} |\dot{\psi}_t^\omega\rangle = (E_t^\omega - H + i\nu) e^{-i\nu} |\psi_t^\omega\rangle \quad (24)$$

and division by $e^{-i\nu}$ leads to

$$|\dot{\psi}_t^\omega\rangle = (E_t^\omega - H + i\nu) |\psi_t^\omega\rangle. \quad (25)$$

Application of McLachlan's variational principle gives

$$\delta \left\| |\dot{\psi}_t^\omega\rangle - (E_t^\omega - H + i\nu) |\psi_t^\omega\rangle \right\|_2 = 0. \quad (26)$$

Next, we evaluate the variational principle with respect to $\dot{\nu}$

$$\delta_{\dot{\nu}} \left\| |\dot{\psi}_t^\omega\rangle - (E_t^\omega - H + i\nu) |\psi_t^\omega\rangle \right\|_2 = 0 \quad (27)$$

and find that $\dot{\nu} = -\text{Im}(\langle \dot{\psi}_t^\omega | \psi_t^\omega \rangle)$. This facilitates a variational time evolution of $|\psi_t^\omega\rangle$ that simulates a global phase degree of freedom ν without actual implementation of $e^{-i\nu}$, i.e.,

$$|\dot{\psi}_t^\nu\rangle = (E_t^\omega - H) |\psi_t^\omega\rangle \quad (28)$$

with the effective state gradient

$$|\dot{\psi}_t^\nu\rangle := |\dot{\psi}_t^\omega\rangle + i\text{Im}(\langle \dot{\psi}_t^\omega | \psi_t^\omega \rangle) |\psi_t^\omega\rangle. \quad (29)$$

Rewriting the variational principle accordingly gives

$$\delta \left\| |\dot{\psi}_t^\nu\rangle - (E_t^\omega - H) |\psi_t^\omega\rangle \right\|_2 = 0. \quad (30)$$

Since the time-dependence of $|\psi_t^\omega\rangle$ is encoded in the parameters ω , Eq. (30) leads to the following system of linear equations

$$\sum_{j=0}^k \mathcal{F}_{ij}^Q \dot{\omega}_j = -\text{Re}(C_i). \quad (31)$$

Further details on the evaluation of the terms in Eq. (31) are given in Appendix E. Solving Eq. (31) for $\dot{\omega}$ leads to an ODE which describes the evolution of the ansatz parameters with respect to Eq. (28)

$$f_{\text{std}}(\omega) = -(\mathcal{F}^Q)^{-1} \text{Re}(C_i). \quad (32)$$

As for VarQRTE, the state gradients may be inexact such that $\| |e_t\rangle \| > 0$ for the gradient error

$$|e_t\rangle := |\dot{\psi}_t^\nu\rangle - (E_t^\omega - H) |\psi_t^\omega\rangle. \quad (33)$$

Eq. (33) motivates alternative VarQITE ODE which is given as the following optimization problem

$$f_{\text{min}}(\omega) = \underset{\omega \in \mathbb{R}^{k+1}}{\text{argmin}} \| |e_t\rangle \|_2^2, \quad (34)$$

for

$$\| |e_t\rangle \|_2^2 = \text{Var}(H)_{\psi_t^\omega} + \langle \dot{\psi}_t^\omega | \dot{\psi}_t^\omega \rangle - \langle \dot{\psi}_t^\omega | \psi_t^\omega \rangle \langle \psi_t^\omega | \dot{\psi}_t^\omega \rangle + 2\text{Re}(\langle \dot{\psi}_t^\omega | H | \psi_t^\omega \rangle), \quad (35)$$

with

$$2\text{Re}(\langle \dot{\psi}_t^\omega | \dot{\psi}_t^\omega \rangle) = \frac{\partial \langle \dot{\psi}_t^\omega | \dot{\psi}_t^\omega \rangle}{\partial t} = 0. \quad (36)$$

Since the time-dependence of $|\psi_t^\omega\rangle$ is encoded in the parameters ω , we can rewrite Eq. (35)

$$\| |e_t\rangle \|_2^2 = \text{Var}(H)_{\psi_t^\omega} + \sum_{i,j} \dot{\omega}_i \dot{\omega}_j \mathcal{F}_{ij}^Q + 2 \sum_i \dot{\omega}_i \text{Re}(C_i),$$

where it is used that

$$\text{Re}(\langle \dot{\psi}_t^\omega | H | \psi_t^\omega \rangle) = \sum_i \dot{\omega}_i \text{Re}(C_i), \quad (37)$$

as well as Eq. (19). This facilitates the efficient evaluation of $\| |e_t\rangle \|_2^2$.

III. ERROR BOUNDS

In this section, we prove new error bounds for VarQTE. Let $|\psi_t^\omega\rangle$ be the state prepared by the variational algorithm at time t and denote the ideal target state by $|\psi_t^*\rangle$. To formalize an error bound, we want to use a metric which describes the distance between two quantum states. A popular distance measure is the fidelity [22] given by $|\langle \psi_t^\omega | \psi_t^* \rangle|^2$. Unlike the ℓ_2 -norm, the fidelity is invariant to changes in the global phases. Since the global phase is physically irrelevant, this is a desired property for a meaningful quantum state distance measure. Although the fidelity itself does not correspond to a metric, it may be used to define metrics such as the Bures metric [23] defined as

$$B(|\psi_t^\omega\rangle\langle\psi_t^\omega|, |\psi_t^*\rangle\langle\psi_t^*|) = \frac{\sqrt{\langle \psi_t^\omega | \psi_t^\omega \rangle + \langle \psi_t^* | \psi_t^* \rangle - 2|\langle \psi_t^\omega | \psi_t^* \rangle|}}{2}, \quad (38)$$

where the states $|\psi_t^\omega\rangle$ and $|\psi_t^*\rangle$ are not necessarily normalized. If the states are normalized then the Bures metric simplifies to

$$B(|\psi_t^\omega\rangle\langle\psi_t^\omega|, |\psi_t^*\rangle\langle\psi_t^*|) = \sqrt{2 - 2|\langle \psi_t^\omega | \psi_t^* \rangle|} = \min_{\phi \in [0, 2\pi]} \| e^{i\phi} |\psi_t^\omega\rangle - |\psi_t^*\rangle \|_2. \quad (39)$$

Unlike the ℓ_2 -norm, the Bures metric is invariant to changes in the global phases.

Our goal is, now, to prove a bound of the form

$$B(|\psi_t^\omega\rangle\langle\psi_t^\omega|, |\psi_t^*\rangle\langle\psi_t^*|) \leq \epsilon_t, \quad (40)$$

for an error term ϵ_t that can be evaluated efficiently in practice. We would again like to point out the aforementioned relation of the Bures metric to the fidelity, which also can be written as

$$|\langle \psi_t^\omega | \psi_t^* \rangle|^2 \geq 1 - \frac{\epsilon_t^2}{2}, \quad (41)$$

and which implies that the relevant range of ϵ_t is $\epsilon_t \in [0, \sqrt{2}]$ for normalized $|\psi_t^\omega\rangle$ and $|\psi_t^*\rangle$. If the error bound estimate lies outside of this interval, then the fidelity and error can be clipped to 0 and $\sqrt{2}$, respectively.

A. Variational Quantum Real Time Evolution

An error bound for VarQRTE in terms of the ℓ_2 -norm has been derived in [11]. We extend this bound to the Bures metric and, thereby, avoid that a physically irrelevant mismatch in the global phase influences the bound. The proof is given in Appendix A.

Theorem 1. *For $T > 0$, let $|\psi_T^*\rangle$ be the exact solution to Eq. (10) and $|\psi_T^\omega\rangle$ correspond to the VarQRTE approximation. Then*

$$B(|\psi_T^*\rangle\langle\psi_T^*|, |\psi_T^\omega\rangle\langle\psi_T^\omega|) \leq \epsilon_T, \quad (42)$$

for $\epsilon_T = \int_0^T \dot{\epsilon}_t dt$ with the error rate given by the gradient error, i.e.,

$$\dot{\epsilon}_t = \| |e_t\rangle \|_2. \quad (43)$$

It should be noted that the error bound is compatible with practical VarQRTE implementations which use, e.g., regularized least squares methods or pseudo-inversion methods to solve the system of linear equations from Eq. (12).

B. Variational Quantum Imaginary Time Evolution

This section introduces an upper-bound to the Bures metric between the target state $|\psi_t^*\rangle$ given by Eq. (20) and $|\psi_t^\omega\rangle$ prepared with VarQITE.

To prove the error bound we need two preparatory lemmas. The first one quantifies the energy difference between E_t^ω and E_t^* . The proof is given in Appendix B.

Lemma 2 (Energy difference). *For $t > 0$, let $|\psi_t^*\rangle$ be the exact solution to Eq. (28) and $|\psi_t^\omega\rangle$ be the variationally prepared state. Suppose that*

$$B(|\psi_t^*\rangle\langle\psi_t^*|, |\psi_t^\omega\rangle\langle\psi_t^\omega|) \leq \epsilon_t, \quad (44)$$

then, $|E_t^\omega - E_t^*| \leq \zeta(\omega_t, \epsilon_t)$ for

$$\zeta(\omega_t, \epsilon_t) = \epsilon_t^2 \|H\|_\infty + 2 \max_{\alpha \in [0, \min\{\epsilon_t^2/2, 1\}]} \left| \alpha E_t^\omega - \sqrt{1 - (1 - \alpha)^2} \sqrt{\text{Var}(H)_{\psi_t^\omega}} \right|. \quad (45)$$

In practice, $\|H\|_\infty$ may be replaced with an efficient approximation thereof. The second Lemma is proven in Appendix C. To shorten the notation, we use $\langle H^2 \rangle := \langle \psi_t^\omega | H^2 | \psi_t^\omega \rangle$.

Lemma 3. *For sufficiently small δ_t such that terms of order $\mathcal{O}(\delta_t^2)$ are negligible, we can upper bound*

$$\begin{cases} \max_{|\psi_t^* \rangle} B((\mathbb{1} + \delta_t(E_t^\omega - H)) |\psi_t^\omega \rangle, (\mathbb{1} + \delta_t(E_t^\omega - H)) |\psi_t^* \rangle) \\ \text{s.t. } \langle \psi_t^* | \psi_t^* \rangle = 1 \ \& \ B(|\psi_t^\omega \rangle, |\psi_t^* \rangle) \leq \varepsilon_t \end{cases} \quad (46)$$

with

$$\sqrt{2 + 2\delta_t \zeta(\boldsymbol{\omega}_t, \epsilon_t) - 2\chi(\boldsymbol{\omega}_t, \epsilon_t)}, \quad (47)$$

where $\zeta(\boldsymbol{\omega}_t, \epsilon_t)$ is defined in (45) and

$$\chi(\boldsymbol{\omega}_t, \epsilon_t) = \begin{cases} \min_{\alpha \in [-1, 1]} \frac{1}{c_\alpha} |(1 + 2\delta_t E_t^\omega)(1 - |\alpha| + \alpha E_t^\omega) \\ \quad - 2\delta_t((1 - |\alpha|)E_t^\omega + \alpha \langle H^2 \rangle)| \\ \text{s.t. } |1 - |\alpha| + \alpha E_t^\omega| \geq c_\alpha(1 - \frac{\varepsilon_t^2}{2}), \end{cases} \quad (48)$$

where

$$c_\alpha = \sqrt{(1 - |\alpha|)^2 + 2\alpha(1 - |\alpha|)E_t^\omega + \alpha^2 \langle H^2 \rangle}. \quad (49)$$

The optimization problems given in Eqs. (45) and (48) can be solved efficiently in practice as they correspond to a one-dimensional search over a closed interval. Furthermore, we would like to point out that $\chi(\boldsymbol{\omega}_t, \epsilon_t)$ bounds the overlap between the two arguments of the objective function in Eq. (46).

We are finally ready to state the error bound for VarQITE. The proof is given in Appendix D.

Theorem 4. *For $T > 0$ and $\varepsilon_0 = 0$, let $|\psi_T^* \rangle$ be the exact solution to Eq. (28) and $|\psi_T^\omega \rangle$ be the simulation implemented using VarQITE. Then*

$$B(|\psi_T^* \rangle \langle \psi_T^*|, |\psi_T^\omega \rangle \langle \psi_T^\omega|) \leq \varepsilon_T, \quad (50)$$

for $\varepsilon_T = \int_0^T \dot{\varepsilon}_t dt$, where

$$\begin{aligned} \varepsilon_{t+\delta_t} &= \delta_t \| |e_t \rangle \|_2 + \delta_t \zeta(\boldsymbol{\omega}_t, \epsilon_t) \\ &\quad + \sqrt{2 + 2\delta_t \zeta(\boldsymbol{\omega}_t, \epsilon_t) - 2\chi(\boldsymbol{\omega}_t, \epsilon_t)}, \end{aligned} \quad (51)$$

with $\zeta(\boldsymbol{\omega}_t, \epsilon_t)$ and $\chi(\boldsymbol{\omega}_t, \epsilon_t)$ as given in Eq. (45) and Eq. (48), respectively, allows to define

$$\begin{aligned} \dot{\varepsilon}_t &= \lim_{\delta_t \rightarrow 0} \frac{\varepsilon_{t+\delta_t} - \varepsilon_t}{\delta_t} \\ &= \| |e_t \rangle \|_2 + \zeta(\boldsymbol{\omega}_t, \epsilon_t) \\ &\quad + \lim_{\delta_t \rightarrow 0} \frac{\sqrt{2 + 2\delta_t \zeta(\boldsymbol{\omega}_t, \epsilon_t) - 2\chi(\boldsymbol{\omega}_t, \epsilon_t)} - \varepsilon_t}{\delta_t}. \end{aligned} \quad (52)$$

This error bound is also independent of a potential physically irrelevant global phase mismatch between prepared and target state. Furthermore, the bound is compatible with implementations which use numerical techniques to solve the SLE given in Eq. (31). Moreover, we

would like to point out that the more complex form of the VarQITE error bound – in comparison to the VarQRTE error bound – is due to the non-unitary nature of imaginary time evolution.

IV. IMPLEMENTATION

To ensure a stable VarQTE implementation, it is vital to choose the correct settings. The possible choices with their advantages and disadvantages, respectively, are explained next.

A. ODE Solvers

The ODE underlying VarQTE is solved using numerical integration. This can lead to an additional error term.

Let $|\psi_t^* \rangle$ denote the target state, $|\psi_t^\omega \rangle$ the prepared state, and $|\psi_t' \rangle$ the state that we would prepare if we could take infinitesimally small time steps and, thus, integrate the ODE exactly. Then, the error bounds derived in Sec. III capture the errors induced by the variational method, i.e.,

$$B(|\psi_t^* \rangle \langle \psi_t^*|, |\psi_t' \rangle \langle \psi_t'|) \leq \epsilon_t. \quad (53)$$

The triangle inequality gives

$$\begin{aligned} B(|\psi_t^* \rangle \langle \psi_t^*|, |\psi_t^\omega \rangle \langle \psi_t^\omega|) &\leq B(|\psi_t^* \rangle \langle \psi_t^*|, |\psi_t' \rangle \langle \psi_t'|) \\ &\quad + B(|\psi_t' \rangle \langle \psi_t'|, |\psi_t^\omega \rangle \langle \psi_t^\omega|). \end{aligned} \quad (54)$$

The term $B(|\psi_t' \rangle \langle \psi_t'|, |\psi_t^\omega \rangle \langle \psi_t^\omega|)$ is generally unknown and the error bounds from Sec. III only hold if $B(|\psi_t' \rangle \langle \psi_t'|, |\psi_t^\omega \rangle \langle \psi_t^\omega|) \ll 1$ such that

$$B(|\psi_t^* \rangle \langle \psi_t^*|, |\psi_t^\omega \rangle \langle \psi_t^\omega|) \approx B(|\psi_t^* \rangle \langle \psi_t^*|, |\psi_t' \rangle \langle \psi_t'|) \leq \epsilon_t. \quad (55)$$

ODE solvers, such as the *forward Euler* method, which operate with a fixed step size may induce large errors in the numerical simulations if the time steps are not chosen sufficiently small. The forward Euler method evaluates the gradient $\dot{\boldsymbol{\omega}}_t$ and propagates the underlying variable for n_T time steps according to a predefined step size, i.e.,

$$\boldsymbol{\omega}_T = \boldsymbol{\omega}_0 + \sum_{k=0}^{n_T} \delta_t \dot{\boldsymbol{\omega}}_{t_k} \quad (56)$$

with $t_{n_T} = T$ and the step-size $\delta_t = t_{k+1} - t_k$. In contrast, *Runge-Kutta* methods evaluate additional supporting points and compute a parameter update using an average of these points, thereby, truncating the local update error. Combining two Runge-Kutta methods of different order but using the same supporting points allows to define efficient adaptive step-size ODE solvers which ensure that the local step-by-step error is small and, thus, that the dominant part of the error is coming from the variational approximation. The results in Sec. V illustrate this

aspect on the example of the forward Euler method [24] with fixed step size and an explicit Runge-Kutta method of order 5(4) (RK54) method from SciPy [25] that uses additional interpolation points as well as an adaptive step size to minimize the step-by-step integration errors. We refer the interested reader to an introductory book on numerical ODE solvers such as [26].

B. ODE Definition

The SLE underlying McLachlan’s variational principle, given in Eq. (12) and Eq. (31), are prone to being ill-conditioned and may, thus, only be solvable approximately with a numerical technique such as regularized least squares or pseudo-inversion. The commonly used regularization schemes, as well as, the pseudo-inversion can be seen as small perturbations which are not necessarily in accordance with the physics of the system. This in turn can lead to inappropriate parameter updates. In the following, we shall refer to the ODE definition based on f_{std} as *standard ODE*. The alternative ODE definition f_{min} – which shall be referred to as *argmin ODE* – is analytically equivalent to solving f_{std} with a least square solver. However, the simulation results in Sec. V show that the numerical behavior differs. In fact, the experiments reveal that the argmin ODE can lead to significantly better numerical stability.

The simulations employ the SciPy COBYLA optimizer [25] to find $\hat{\omega}$ in f_{min} where the initial point is chosen as the numerical solution to the SLE given in Eq. (12) and Eq. (31), respectively.

C. Error Bound Evaluation

To enable a reliable error bound evaluation, we jointly evolve the state parameters and the error bounds. More explicitly, we extend the parameter ODE to

$$\begin{pmatrix} \dot{\omega}_t \\ \dot{\epsilon}_t \end{pmatrix} = \tilde{f}(\omega_t, \epsilon_t), \quad (57)$$

with ω_0 being set, $\epsilon_0 = 0$ by assumption, and

$$\tilde{f}(\omega_t, \epsilon_t) = \begin{pmatrix} f(\omega_t) \\ \dot{\epsilon}_t \end{pmatrix}, \quad (58)$$

with $\dot{\epsilon}_t$ from Eqs. (43) and (52) for the real and imaginary case, respectively. Furthermore, $f(\omega_t)$ is either chosen as $f_{\text{std}}(\omega_t)$ or $f_{\text{min}}(\omega_t)$. Note, that we need to use a finite difference approximation to evaluate $\dot{\epsilon}_t$ for VarQITE, i.e., we evaluate $\epsilon_{t+\delta_t}$ for a small $\delta_t > 0$ – which is independent of the ODE solver’s step size – according to Eq. (51). This formulation has the advantage that the error bound directly reflects the propagation of the evolution and that adaptive step size ODE solvers also consider the changes in the error bounds.

V. SIMULATION RESULTS

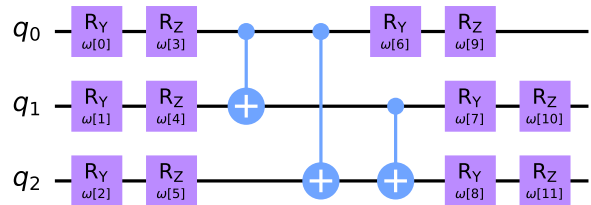


FIG. 1 This quantum circuit corresponds to the *EfficientSU2* ansatz in Qiskit’s [27] circuit library and is chosen as ansatz for the experiments presented in this work. It consists of layers of R_Y and R_Z rotations and a CX entanglement block which is chosen according to the *full* layout. The number of repetitions is set to 1.

We next introduce three examples that we will use to demonstrate the efficiency of the error bounds derived in Sec. III, as well as, the impact of the implementation details discussed in Sec. IV. All experiments prepare $|\psi_t^\omega\rangle$ with an ansatz as shown in Fig. 1, adjusted to the number of qubits n given by the respective Hamiltonian:

- (i) An illustrative example is considered with

$$H_{\text{illustrative}} = Z \otimes X + X \otimes Z + 3Z \otimes Z. \quad (59)$$

Hereby, the evolution time is $T = 1$ and the initial parameters are chosen such that all parameters are set to 0 except for the parameters of the last layer of R_Y rotations which are chosen to be $\pi/2$. This gives $|\psi_0\rangle = |++\rangle$.

- (ii) The well-studied Ising model with a transverse magnetic field on an open chain with 3 qubits is investigated, see, e.g., [28], i.e.,

$$H_{\text{Ising}} = -J \left(\sum_{i,j} Z_i \otimes Z_j + g \sum_j X_j \right), \quad (60)$$

where $J = -\frac{1}{2}$ and $g = -\frac{1}{2}$. The evolution time is again set to $T = 1$ and the initial parameters are all 0 except for the parameters of the last layer of R_Z gates which are chosen at random in $(0, \frac{\pi}{2}]$ such that $|\psi_0\rangle = e^{-i\gamma} |000\rangle$ with $\gamma \in \mathbb{R}$. Notably, we avoid the initial state $|\psi_0\rangle = |000\rangle$ to circumvent getting stuck in a local minima.

- (iii) The two qubit hydrogen molecule approximation given in [9] is studied, with

$$\begin{aligned} H_{\text{hydrogen}} = & 0.2252 I \otimes I + 0.5716 Z \otimes Z \\ & + 0.3435 I \otimes Z - 0.4347 Z \otimes I \\ & + 0.0910 Y \otimes Y + 0.0910 X \otimes X. \end{aligned} \quad (61)$$

Again, the evolution time is set to $T = 1$ and the initial parameters are chosen such that the initial state is $|\psi_0\rangle = |++\rangle$, i.e., all parameters are 0 except for the last layer of R_Y rotations which are given as $\pi/2$.

A. Variational Quantum Real Time Evolution

VarQRTE: $H_{\text{illustrative}}$ with different ODE solvers

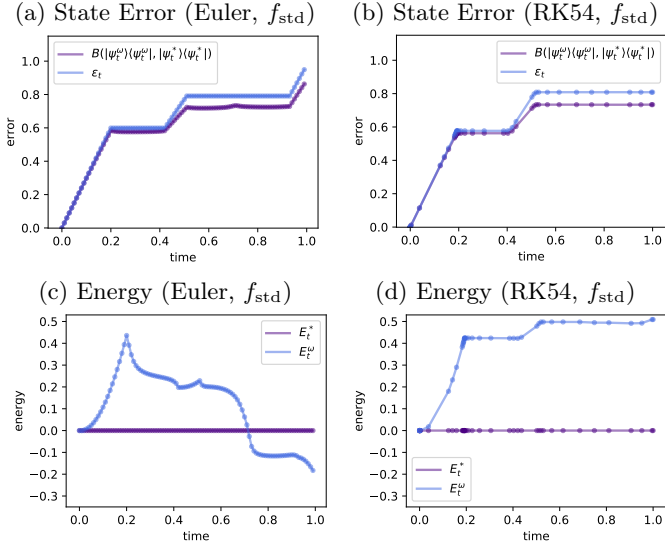


FIG. 2 VarQRTE for $|\psi_0\rangle = |++\rangle$, $H_{\text{illustrative}}$ and $T = 1$ with the standard ODE. (a), (c) employ forward Euler. (b), (d) use RK54. - (a), (b) illustrate the error bounds ϵ_t and the actual Bures metric between $|\psi_t^*\rangle$ and $|\psi_t^\omega\rangle$. (c), (d) show the corresponding energies.

In the following, we present a set of numerical experiments and investigate the error bounds for VarQRTE with a particular focus on the comparison of different ODE formulations and solvers.

Firstly, we apply the forward Euler method with 100 time steps as well as an adaptive step size RK54 ODE solver to the illustrative example using the standard ODE. The resulting SLEs are solved using a least square solver provided by NumPy [29]. The results shown in Fig. 2 illustrate that the error bounds are very tight and, thus, relevant for practical accuracy estimations. Furthermore, one can see that RK54 achieves better error bounds as well as smaller fluctuations in the system energy while using significantly less time steps. The plateaus are due to exact local gradients, i.e., $\| |e_t\rangle \|_2 = 0$. Furthermore, we would like to point out that the energy should actually be preserved for a real time evolution under a time-independent Hamiltonian but McLachlan's variational principle does not guarantee energy preservation.

Next, we compare the implications of the ODE formulation on the Ising model using RK54. The initial points

VarQRTE: H_{Ising} with different ODE definitions

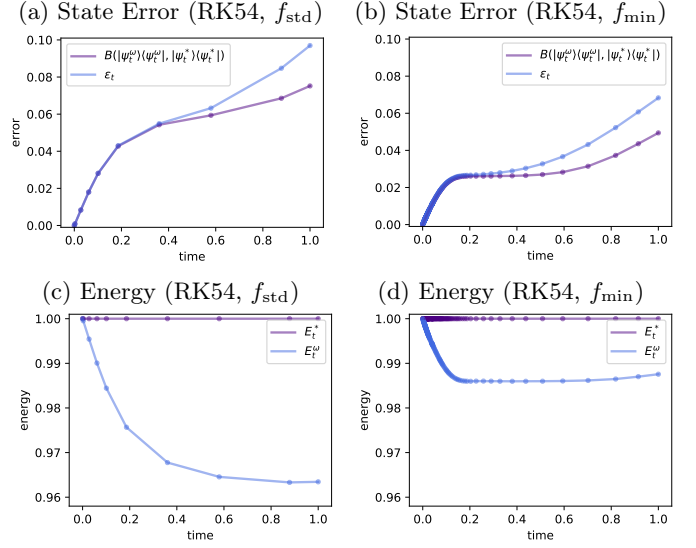


FIG. 3 VarQRTE for $|\psi_0\rangle = e^{-i\alpha} |000\rangle$, H_{Ising} and $T = 1$ with RK54. (a), (c) are based on the standard ODE. (b), (d) use the argmin ODE. - (a), (b) illustrate the error bounds ϵ_t and the actual Bures metrics corresponding to prepared and target state.

for the optimization of the argmin ODE are chosen as the solution to the respective SLE at time t . Fig. 3 presents the Bures metrics, as well as, the respective bounds for the prepared $|\psi_t^\omega\rangle$ and the target state $|\psi_t^*\rangle$. The errors show that the argmin ODE leads to smaller errors than the standard ODE. Furthermore, it can be seen that also the system energy changes less for the former.

Lastly, the error bounds for the hydrogen Hamiltonian from Eq. (61) are compared the standard and argmin ODE as well as forward Euler and RK54 ODE solvers. The results are presented in Fig. 4. Notably, the experiment which uses RK54 and the argmin ODE leads to the best results, i.e., the smallest state error as well as error bound. In general, one can see that the argmin ODE achieves better errors compared to the standard ODE, the error seems to saturate for the former while it keeps increasing with the latter. Furthermore, RK54 improves the errors, as well as, the error bounds for both ODE definitions while using significantly less time steps. We would like to point out that the setting which gives to the smallest error ϵ_t does not necessarily lead to the smallest discrepancy between E_t^ω and E_t^* , as can be seen when comparing the RK54 results.

To sum this up, the numerical results reveal that the error bounds represent good estimates for the actual errors. The experiments indicate further that an adaptive step size ODE solver such as RK54 significantly improves the simulation results while reducing the computational costs. Moreover, it was shown that replacing the standard ODE by the argmin ODE has also a positive influence on the simulation accuracy. Lastly, the results

VarQRTE: H_{hydrogen} with different ODE solvers and different ODE types

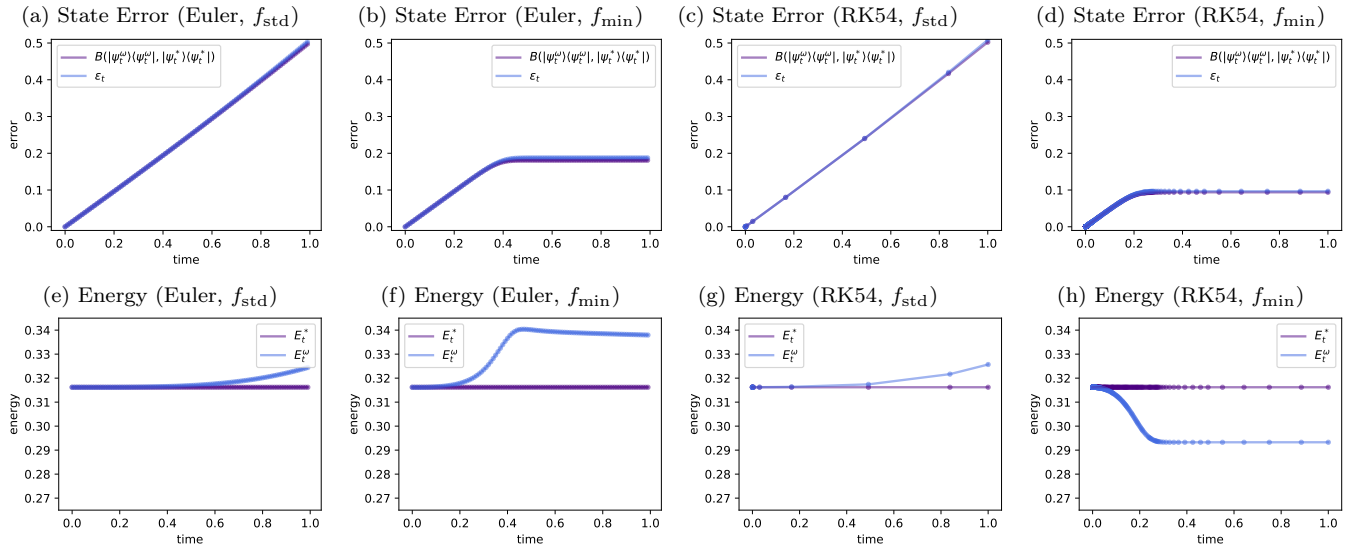


FIG. 4 VarQRTE for $|\psi_0\rangle = |++\rangle$, H_{hydrogen} and $T = 1$. (a), (b), (e), (f) employ a forward Euler solver. (c), (d), (g), (h) use an RK54 ODE solver. (a), (c), (e), (g) use the standard ODE. (b), (d), (f), (h) rely on the argmin ODE. - (a), (b), (c), (d) illustrate the error bounds ϵ_t and the true Bures metric. (e), (f), (g), (h) show the respective energies E_t^ω and E_t^* .

reveal that the lack of energy conservation in McLachlan’s variational principle can lead to significant energy fluctuations.

B. Variational Quantum Imaginary Time Evolution

Next, we investigate the power of the error bounds for VarQITE. To that end, the optimizations for $\zeta(\omega_t, \epsilon_t)$ and $\chi(\omega_t, \epsilon_t)$, see Lemmas 2 and 3, respectively, use a grid search which is viable since the problems are cheap to evaluate. Furthermore, we would like to point out that δ_t , used to compute $\hat{\epsilon}_t \approx \frac{\epsilon_t - \epsilon_{t-1}}{\delta_t}$, does not need to correspond to the step size of the ODE solver but may be chosen such that a reasonable finite difference approximation is obtained. We set $\delta_t = 10^{-4}$.

First, the outcomes using the standard ODE with forward Euler as well as RK54 are compared for $H_{\text{illustrative}}$. The results shown in Fig. 5 provide an example of the potentially insufficient numerical integration accuracy of forward Euler. More explicitly, although the gradient errors and, thus, also the error bounds are all 0, the actual error between prepared and target state, i.e., $B(|\psi_T^*\rangle\langle\psi_T^*|, |\psi_t^\omega\rangle\langle\psi_t^\omega|)$, shown in purple, is positive. The application of RK54 in comparison reduces the error in the integration. Furthermore, the plotted energies E_t^ω and E_t^* are very close and show a convergence behavior. Since the state error is sufficiently small and the energy variance $\text{Var}(H)_{\psi_t^\omega} = \langle\psi_t^\omega|H^2|\psi_t^\omega\rangle - (E_t^\omega)^2$ shown in Fig. 5 (d), (h) converges to 0, we can conclude that the VarQITE is run for a sufficiently long time and actually reached the ground state.

Moreover, the performance using RK54 and the stan-

dard respectively argmin ODE formulation is compared on the example of H_{Ising} . Fig. 6 illustrates the sensitivity of the error bounds for VarQITE with respect to the gradient errors $\| |e_t\rangle \|_2$. Since the gradient errors are rather large especially at the beginning of the evolution, the error bounds reach the maximum value of $\sqrt{2}$. At this point, they are not representative for the actual error $B(|\psi_T^*\rangle\langle\psi_T^*|, |\psi_t^\omega\rangle\langle\psi_t^\omega|)$ anymore. Notably, for this example the argmin ODE only works marginally better than the standard ODE.

For VarQITE applied to H_{hydrogen} , we focus on RK54 and the argmin ODE formulation. The results are visualized in Fig. 7. The SLE is solved with a least squares method from NumPy [29]. It can be seen that VarQITE is able to represent the state exactly and that all gradient errors $\| |e_t\rangle \|_2$ are 0. This is directly reflected by the respective error bound ϵ_t and fidelity bound $(1 - \epsilon_t^2/2)^2$. Furthermore, the energy with respect to the prepared state E_t^ω is equal to E_t^* at all times of the numerical ODE integration.

The presented experiments show that the error bounds are good approximations to the actual error if the gradient errors are small. In the case of larger gradient errors, the error bounds can grow fast and exceed the meaningful range. Moreover, the results reveal that the numerical integration error introduced by Forward Euler can easily exceed the error bounds, rendering them useless.

VI. CONCLUSION AND OUTLOOK

This work presents a posteriori error bounds for the Bures metric between a state prepared with VarQITE

VarQITE: $H_{\text{illustrative}}$ with different ODE solvers

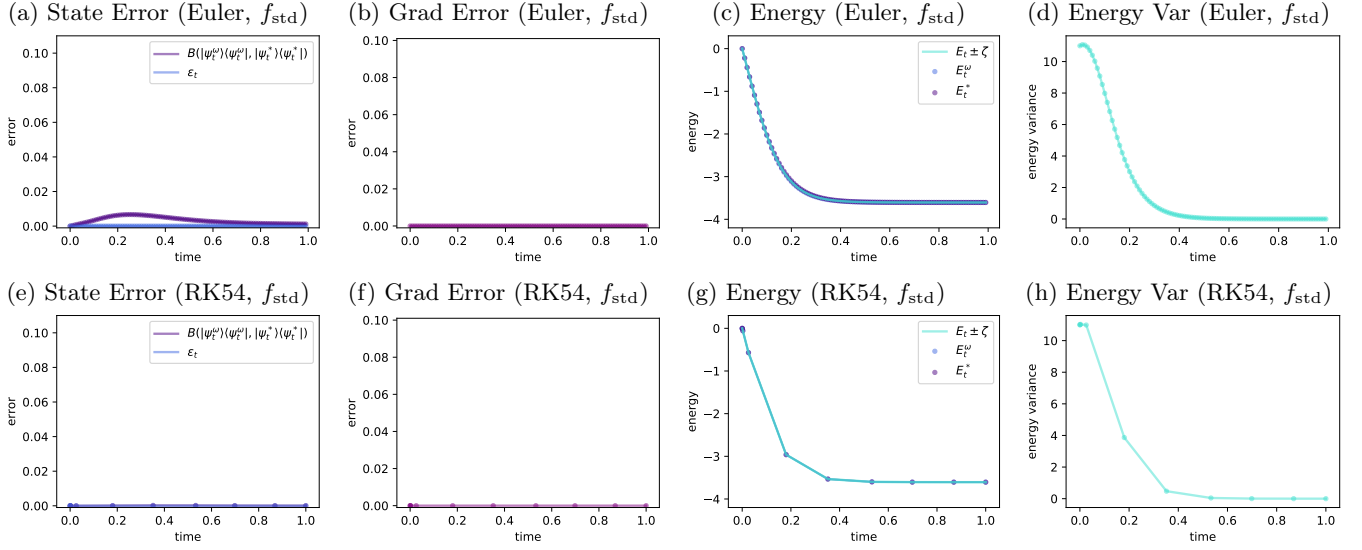


FIG. 5 VarQITE for $|\psi_0\rangle = |++\rangle$, $H_{\text{illustrative}}$ and $T = 1$ with the standard ODE (a), (b), (c), (d) are computed using Forward Euler. (e), (f), (g), (h) employ RK54. - (a), (e) illustrate the error bound ϵ_t and the true Bures metric. Furthermore, (b), (f) show the gradient errors $\| |e_t\rangle \|_2$. (c), (g) present the energies E_t^ω and E_t^* , as well as, the error bound to E_t^ω , i.e., $E_t^\omega \pm \zeta(\omega_t, \epsilon_t)$. Lastly, (d), (h) present the evolution of the energy variance $\text{Var}(H)_{\psi_t^\omega}$.

VarQITE: H_{Ising} with different ODE definitions

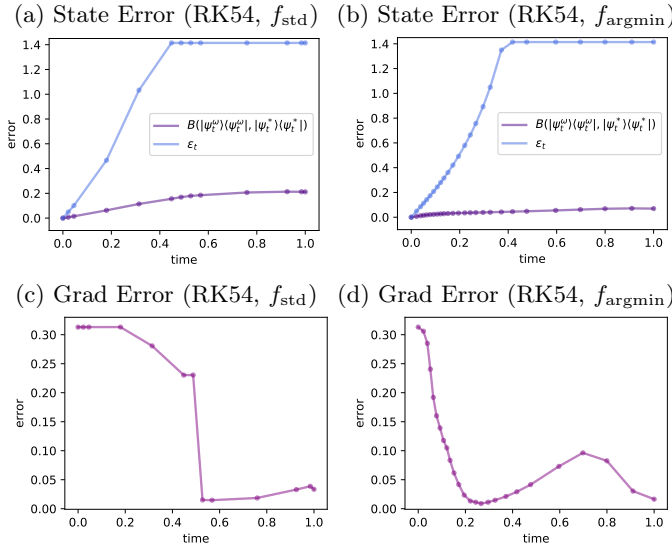


FIG. 6 VarQITE for $|\psi_0\rangle = e^{-i\gamma} |000\rangle$, H_{Ising} and $T = 1$ with RK54. (a), (b) employ the standard ODE. (c), (d) use the argmin ODE. (a), (c) illustrate the error bound ϵ_t , as well as, the actual Bures metric. (b), (d) present the corresponding evolution of the gradient errors $\| |e_t\rangle \|_2$.

and the respective unknown target state resulting from exact QTE. These bounds enable users to quantify the accuracy of their quantum time evolution simulation and potentially adapt their simulation setting if necessary.

The presented error bound for VarQRTE extends a

VarQITE: H_{hydrogen}

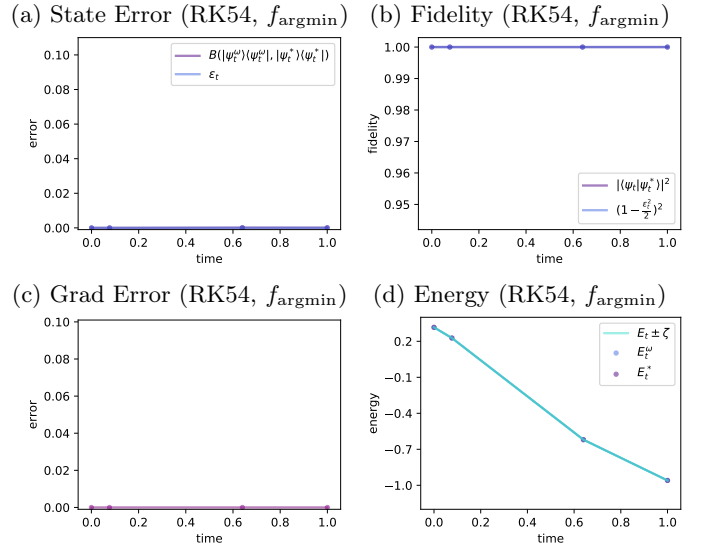


FIG. 7 VarQITE for $|\psi_0\rangle = |++\rangle$, H_{hydrogen} and $T = 1$. All plots are based on RK54 and the argmin ODE. - (a) illustrates the error bound ϵ_t , as well as, the actual Bures metric. (b) shows the corresponding fidelity bound $(1 + \epsilon^2/2)^2$, as well as, the actual fidelity $|\langle \psi_t^\omega | \psi_t^* \rangle|^2$. Furthermore, (c) illustrates the evolution of the gradient errors $\| |e_t\rangle \|_2$. (d) presents the system energy E_t^ω corresponding to the prepared state, the energy E_t^* corresponding to the target state and the error bound to E_t^ω , i.e., $E_t^\omega \pm \zeta(\omega_t, \epsilon_t)$.

known error bound [11] to be independent of a physically irrelevant global phase – a property that is important for

practical applications. Furthermore, the novel bound is particularly simple to evaluate.

The error bound for VarQITE, on the other hand, is more involved as it implicates solving two constrained optimization problems but can still be evaluated efficiently. The complexity of this error bound is largely due to the non-unitary characteristics of imaginary time evolution. The presented error bounds are insightful whenever the errors at the individual time steps remain sufficiently small. Otherwise, the error bounds can grow quite fast and lose their informative value. We leave it for future work to derive error bounds that are applicable for larger errors.

We argue and verify numerically that the error bounds are strongly dependent on the numerical integration method. An ODE solver which applies an adaptive step size scheme can increase the numerical stability and accuracy significantly. Furthermore, using an ODE formulation which is based on the minimization of the local gradient error $\|e_t\|_2$ also helps to reduce the simulation errors. The performance of the algorithm, the error bounds, related state fidelities, and system energies, are demonstrated on numerical examples.

An open question for future investigation, is the influence of quantum hardware noise on these error bounds. The device noise impacts the components used to evaluate the error bounds, as well as, the parameter updates. It is particularly interesting to what extent the error bounds are robust given a noisy sampling process. Moreover, we expect that a focused investigation of the behavior of VarQTE and the respective error bounds at critical points, such as phase transitions, can give us important insights into the limits and potentials of the QTE simulation technique. Finally, we suggest the application of physically motivated regularization methods, e.g., with respect to the changes in the system energy, instead of the standard regularization techniques which do not necessarily lead to physically relevant results.

Acknowledgments. We thank Pauline Ollitrault, Alexander Miessen, and Guglielmo Mazzola for insightful discussions on VarQRTE applications and Julien Gacon for proofreading this manuscript. CZ acknowledges support from the National Centre of Competence in Research *Quantum Science and Technology* (QSIT).

Appendix A: Proof of Theorem 1

For $\delta_t > 0$, let the state evolution be defined with respect to the effective gradient given in Eq. (10)

$$\begin{aligned} |\psi_{t+\delta_t}^\omega\rangle &= |\psi_t^\omega\rangle + \delta_t |\dot{\psi}_t^\omega\rangle \\ &= |\psi_t^\omega\rangle + \delta_t \left(|\dot{\psi}_t^\omega\rangle - iE_t^\omega - i\text{Im}(\langle \dot{\psi}_t^\omega | \psi_t^\omega \rangle) |\psi_t^\omega\rangle \right). \end{aligned} \quad (\text{A1})$$

For the remainder of the proof, we use the simplified notation $B(|v\rangle, |w\rangle)$ when referring to $B(|v\rangle\langle v|, |w\rangle\langle w|)$.

Combining Eq. (A1) with the triangle inequality gives

$$\begin{aligned} B(|\psi_{t+\delta_t}^\omega\rangle, |\psi_{t+\delta_t}^*\rangle) &\leq B(|\psi_{t+\delta_t}^\omega\rangle, (\mathbb{1} - i\delta_t H) |\psi_t^\omega\rangle) \\ &\quad + B((\mathbb{1} - i\delta_t H) |\psi_t^\omega\rangle, |\psi_{t+\delta_t}^*\rangle). \end{aligned} \quad (\text{A2})$$

Using Eq. (39) and neglecting terms of order $\mathcal{O}(\delta_t^2)$ gives

$$\begin{aligned} &B(|\psi_{t+\delta_t}^\omega\rangle, (\mathbb{1} - i\delta_t H) |\psi_t^\omega\rangle) \\ &= \min_{\phi \in [0, 2\pi]} \|e^{i\phi} (|\psi_{t+\delta_t}^\omega\rangle) - (\mathbb{1} - i\delta_t H) |\psi_t^\omega\rangle\|_2 \\ &\leq \| |\psi_{t+\delta_t}^\omega\rangle - (\mathbb{1} - i\delta_t H) |\psi_t^\omega\rangle \|_2 \\ &= \delta_t \left\| |\dot{\psi}_t^\omega\rangle + i(H - E_t^\omega - \text{Im}(\langle \dot{\psi}_t^\omega | \psi_t^\omega \rangle)) |\psi_t^\omega\rangle \right\|_2 \\ &=: \delta_t \|e_t\|_2, \end{aligned} \quad (\text{A3})$$

where the penultimate step uses Eq. (9).

To bound the second term in Eq. (A2), we again use Eq. (39), neglecting terms of order $\mathcal{O}(\delta_t^2)$ to obtain

$$\begin{aligned} &B((\mathbb{1} - i\delta_t H) |\psi_t^\omega\rangle, (\mathbb{1} - i\delta_t H) |\psi_t^*\rangle) \\ &= \min_{\phi \in [0, 2\pi]} \|(\mathbb{1} - i\delta_t H) (e^{i\phi} |\psi_t^\omega\rangle - |\psi_t^*\rangle)\|_2 \\ &\leq \min_{\phi \in [0, 2\pi]} \|e^{-i\delta_t H} (e^{i\phi} |\psi_t^\omega\rangle - |\psi_t^*\rangle)\|_2 \\ &\quad + \left\| \left((\mathbb{1} - i\delta_t H) - e^{-i\delta_t H} \right) (e^{i\phi} |\psi_t^\omega\rangle - |\psi_t^*\rangle) \right\|_2 \\ &= \min_{\phi \in [0, 2\pi]} \|e^{-i\delta_t H} (e^{i\phi} |\psi_t^\omega\rangle - |\psi_t^*\rangle)\|_2 \\ &= B(|\psi_t^\omega\rangle, |\psi_t^*\rangle). \end{aligned} \quad (\text{A4})$$

The penultimate step uses that $\mathbb{1} - i\delta_t H$ is the first Taylor expansion of $\exp(-i\delta_t H)$ and drops terms of order $\mathcal{O}(\delta_t^2)$.

Combining Eqs (A2), (A3) and (A4) gives

$$B(|\psi_{t+\delta_t}^\omega\rangle, |\psi_{t+\delta_t}^*\rangle) \leq B(|\psi_t^\omega\rangle, |\psi_t^*\rangle) + \delta_t \|e_t\|_2. \quad (\text{A5})$$

Assuming that $B(|\psi_0\rangle, |\psi_0^*\rangle) = 0$, we can evolve

$$B(|\psi_T^\omega\rangle, |\psi_T^*\rangle) = \delta_t \sum_{k=0}^K \|e_{k\delta_t}\|_2, \quad (\text{A6})$$

where K corresponds to the number of time steps. Finally setting $\delta_t = T/t$ leads to

$$B(|\psi_T^\omega\rangle, |\psi_T^*\rangle) \leq \int_0^T \|e_t\|_2 dt := \epsilon_T, \quad (\text{A7})$$

which proves the assertion. \square

Appendix B: Proof of Lemma 2

Let us denote by $\phi \in [0, 2\pi]$ the optimal phase induced by $B(|\psi_t^*\rangle, |\psi_t^\omega\rangle)$ according to Eq. (39) and set $|\psi_t^\phi\rangle =$

$e^{i\phi} |\psi_t^\omega\rangle$. Next, let $|\mathcal{E}_t\rangle := |\psi_t^*\rangle - |\psi_t^\phi\rangle$, which by definition satisfies

$$\| |\mathcal{E}_t\rangle \|_2 = B(|\psi_t^*\rangle, |\psi_t^\omega\rangle) \leq \epsilon_t. \quad (\text{B1})$$

Then,

$$\begin{aligned} |E_t^\omega - E_t^*| &= |\langle \psi_t^\omega | H | \psi_t^\omega \rangle - \langle \psi_t^* | H | \psi_t^* \rangle| \\ &= |\langle \psi_t^\phi | H | \psi_t^\phi \rangle - \langle \psi_t^* | H | \psi_t^* \rangle| \\ &= |\langle \psi_t^\phi | H | \mathcal{E}_t \rangle + \langle \mathcal{E}_t | H | \psi_t^\phi \rangle + \langle \mathcal{E}_t | H | \mathcal{E}_t \rangle| \\ &\leq |\langle \mathcal{E}_t | H | \mathcal{E}_t \rangle| + 2|\langle \mathcal{E}_t | H | \psi_t^\phi \rangle|. \end{aligned} \quad (\text{B2})$$

From Cauchy-Schwarz we find

$$|\langle \mathcal{E}_t | H | \mathcal{E}_t \rangle| \leq \| \mathcal{E}_t \|_2 \| H \mathcal{E}_t \|_2 \leq \epsilon_t^2 \| H \|_\infty. \quad (\text{B3})$$

Furthermore,

$$\begin{aligned} |\langle \mathcal{E}_t | H | \psi_t^\phi \rangle| &= |\langle \psi_t^\phi | H | \psi_t^\phi \rangle - \langle \psi_t^* | H | \psi_t^\phi \rangle| \\ &\leq \begin{cases} \max_{|\psi_t^*} |\langle \psi_t^\phi | H | \psi_t^\phi \rangle - \langle \psi_t^* | H | \psi_t^\phi \rangle| \\ \text{s.t. } \langle \psi_t^* | \psi_t^* \rangle = 1 \\ |\langle \psi_t^\phi | \psi_t^* \rangle| \geq 1 - \epsilon_t^2/2. \end{cases} \end{aligned} \quad (\text{B4})$$

Here, the optimizer $|\psi_t^*\rangle$ can absorb the phase $e^{i\phi}$, and thus, the optimization problem is equivalent to

$$\begin{cases} \max_{|\psi_t^*} |\langle \psi_t^\omega | H | \psi_t^\omega \rangle - \langle \psi_t^* | H | \psi_t^\omega \rangle| \\ \text{s.t. } \langle \psi_t^* | \psi_t^* \rangle = 1 \\ |\langle \psi_t^\omega | \psi_t^* \rangle| \geq 1 - \epsilon_t^2/2, \end{cases} \quad (\text{B5})$$

with the optimizer having the form

$$|\psi_t^*\rangle = (1-\alpha) |\psi_t^\omega\rangle \pm \sqrt{1-(1-\alpha)^2} \frac{(H - E_t^\omega) |\psi_t^\omega\rangle}{\sqrt{\langle \psi_t^\omega | (H - E_t^\omega)^2 | \psi_t^\omega \rangle}} \quad (\text{B6})$$

for $\alpha \in [0, 1]$. Inserting this above and noting that $|\langle \psi_t^\omega | \psi_t^* \rangle| = 1 - \alpha \geq 1 - \epsilon_t^2/2$ proves Eq. (45).

Appendix C: Proof of Lemma 3

We start by noting that

$$\| (\mathbb{1} + \delta_t (E_t^\omega - H)) |\psi_t^\omega\rangle \|_2^2 = 1 + \mathcal{O}(\delta_t^2) \quad (\text{C1})$$

and

$$\begin{aligned} \| (\mathbb{1} + \delta_t (E_t^\omega - H)) |\psi_t^*\rangle \|_2^2 &= 1 + 2\delta_t (E_t^\omega - E_t^*) + \mathcal{O}(\delta_t^2) \\ &\leq 1 + 2\delta_t \zeta(\omega_t, \epsilon_t) + \mathcal{O}(\delta_t^2), \end{aligned} \quad (\text{C2})$$

where the final step uses (45). Furthermore, note that by neglecting terms of order $\mathcal{O}(\delta_t^2)$ we have

$$\begin{aligned} &|\langle \psi_t^\omega | (\mathbb{1} + \delta_t (E_t^\omega - H)) (\mathbb{1} + \delta_t (E_t^\omega - H)) |\psi_t^*\rangle|^2 \\ &= |(\mathbb{1} + 2\delta_t E_t^\omega) \langle \psi_t^\omega | \psi_t^* \rangle - 2\delta_t \langle \psi_t^\omega | H | \psi_t^* \rangle|^2. \end{aligned} \quad (\text{C3})$$

By definition of the Bures metric and neglecting terms of order $\mathcal{O}(\delta_t^2)$, we find

$$(46) \leq \sqrt{2 + 2\delta_t \zeta(\omega_t, \epsilon_t) - 2\xi} \quad (\text{C4})$$

for

$$\xi = \begin{cases} \min_{|\psi_t^*} |(1 + 2\delta_t E_t^\omega) \langle \psi_t^\omega | \psi_t^* \rangle - 2\delta_t \langle \psi_t^\omega | H | \psi_t^* \rangle| \\ \text{s.t. } \langle \psi_t^* | \psi_t^* \rangle = 1 \quad \& \quad |\langle \psi_t^\omega | \psi_t^* \rangle| \geq 1 - \epsilon_t^2/2. \end{cases} \quad (\text{C5})$$

The optimizer for (C5) is of the form

$$|\psi_t^*\rangle = \frac{(1 - |\alpha|) |\psi_t^\omega\rangle + \alpha H |\psi_t^\omega\rangle}{c_\alpha}, \quad \alpha \in [-1, 1]. \quad (\text{C6})$$

Plugging (C6) into (46) shows that $\xi = \chi(\omega_t, \epsilon_t)$ from Eq. (48) because

$$|\langle \psi_t^\omega | \psi_t^* \rangle| = \frac{1}{c_\alpha} (1 - |\alpha| + \alpha E_t^\omega) \quad (\text{C7})$$

and

$$|\langle \psi_t^\omega | H | \psi_t^* \rangle| = \frac{1}{c_\alpha} ((1 - |\alpha|) E_t^\omega + \alpha \langle H^2 \rangle). \quad (\text{C8})$$

This then proves the assertion.

Appendix D: Proof of Theorem 4

For $\delta_t > 0$, Eq. (28) gives

$$\begin{aligned} |\psi_{t+\delta_t}^\omega\rangle &= |\psi_t^\omega\rangle + \delta_t |\dot{\psi}_t^\omega\rangle \\ &= |\psi_t^\omega\rangle + \delta_t \left(|\dot{\psi}_t^\omega\rangle + i \text{Im}(\langle \dot{\psi}_t^\omega | \psi_t^\omega \rangle) |\psi_t^\omega\rangle \right). \end{aligned} \quad (\text{D1})$$

Combining this with the triangle inequality gives

$$\begin{aligned} &B(|\psi_{t+\delta_t}^\omega\rangle, |\psi_{t+\delta_t}^*\rangle) \\ &\leq B(|\psi_t^\omega\rangle + \delta_t |\dot{\psi}_t^\omega\rangle, (\mathbb{1} + \delta_t (E_t^\omega - H)) |\psi_t^\omega\rangle) \\ &\quad + B((\mathbb{1} + \delta_t (E_t^\omega - H)) |\psi_t^\omega\rangle, (\mathbb{1} + \delta_t (E_t^\omega - H)) |\psi_t^*\rangle) \\ &\quad + B((\mathbb{1} + \delta_t (E_t^\omega - H)) |\psi_t^*\rangle, |\psi_{t+\delta_t}^*\rangle). \end{aligned} \quad (\text{D2})$$

We next bound all three terms separately. Using Eq. (39) and neglecting terms of order $\mathcal{O}(\delta_t^2)$ gives

$$\begin{aligned} &B(|\psi_t^\omega\rangle + \delta_t |\dot{\psi}_t^\omega\rangle, (\mathbb{1} + \delta_t (E_t^\omega - H)) |\psi_t^\omega\rangle) \\ &= \min_{\phi \in [0, 2\pi]} \left\| e^{i\phi} (|\psi_t^\omega\rangle + \delta_t |\dot{\psi}_t^\omega\rangle) - (\mathbb{1} + \delta_t (E_t^\omega - H)) |\psi_t^\omega\rangle \right\|_2 \\ &\leq \left\| |\psi_t^\omega\rangle + \delta_t |\dot{\psi}_t^\omega\rangle - (\mathbb{1} + \delta_t (E_t^\omega - H)) |\psi_t^\omega\rangle \right\|_2 \\ &= \delta_t \left\| |\dot{\psi}_t^\omega\rangle - (E_t^\omega - H) |\psi_t^\omega\rangle \right\|_2 \\ &= \delta_t \left\| |\dot{\psi}_t^\omega\rangle - \left(E_t^\omega - H - i \text{Im}(\langle \dot{\psi}_t^\omega | \psi_t^\omega \rangle) \right) |\psi_t^\omega\rangle \right\|_2 \\ &= \delta_t \| |e_t\rangle \|_2, \end{aligned} \quad (\text{D3})$$

where the penultimate step uses Eq. (29).

The second term in Eq. (D2) is bounded from above by Lemma 3. It thus remains to bound the third term in Eq. (D2) With the help of Eq. (39) we find

$$\begin{aligned}
& B\left(\left(\mathbb{1} + \delta_t(E_t^\omega - H)\right) |\psi_t^*\rangle, |\psi_{t+\delta_t}^*\rangle\right) \\
&= \min_{\phi \in [0, 2\pi]} \left\| e^{i\phi} \left(\left(\mathbb{1} + \delta_t(E_t^\omega - H)\right) |\psi_t^*\rangle\right) - |\psi_{t+\delta_t}^*\rangle \right\|_2 \\
&\leq \left\| \left(\mathbb{1} + \delta_t(E_t^\omega - H)\right) |\psi_t^*\rangle - \left(\mathbb{1} + \delta_t(E_t^* - H)\right) |\psi_t^*\rangle \right\|_2 \\
&= \delta_t \left\| (E_t^\omega - E_t^*) |\psi_t^*\rangle \right\|_2 \\
&\leq \delta_t |E_t^\omega - E_t^*| \left\| |\psi_t^*\rangle \right\|_2 \\
&= \delta_t |E_t^\omega - E_t^*| \\
&\leq \delta_t \zeta,
\end{aligned} \tag{D4}$$

where $\zeta(\omega_t, \epsilon_t)$ is defined in Eq. (45). \square

Appendix E: VarQTE Implementation

The implementation of VarQTE relies on the evaluation of $\text{Im}(C_i - \frac{\partial \langle \psi_t^\omega |}{\partial \omega_i} |\psi_t^\omega\rangle E_t^\omega)$, $\text{Re}(C_i)$ and \mathcal{F}_{ij}^Q which are introduced in Sec. II. The parameterized state is constructed as $|\psi_t^\omega\rangle = \prod_{p=0}^k U_p(\omega_p) |0\rangle^{\otimes n}$. Thus, we may use that parameterized unitaries can be written as $U_j(\omega_j) = e^{iM(\omega_j)}$, where $M(\omega_j)$ denotes a parameterized Hermitian matrix. To simplify the notation, we assume that $M(\omega_j) = -\frac{\omega_j}{2} \sigma_j$ for $\sigma_j \in \{1, X, Y, Z\}$. Since

$$\frac{\partial U_j(\omega_j)}{\partial \omega_j} = -\frac{i}{2} \sigma_j U_j(\omega_j), \tag{E1}$$

it follows that

$$\frac{\partial |\psi_t^\omega\rangle}{\partial \omega_j} = -\frac{i}{2} \prod_{p=j+1}^k U_p(\omega_p) \sigma_j U_j(\omega_j) \prod_{p=0}^{j-1} U_p(\omega_p) |0\rangle^{\otimes n}. \tag{E2}$$

Next, we employ Eq. (E2) to find that

$$C_i = -\frac{i}{2} \langle \psi_t^\omega | H \prod_{p=j+1}^k U_p \sigma_j U_j \prod_{p=0}^{j-1} U_p |0\rangle^{\otimes n}, \tag{E3}$$

as well as,

$$\frac{\partial \langle \psi_t^\omega |}{\partial \omega_i} |\psi_t^\omega\rangle = \frac{i}{2} \langle 0 |^{\otimes n} \prod_{p=0}^{j-1} U_p^\dagger U_j^\dagger \sigma_j \prod_{p=j+1}^k U_p^\dagger |\psi_t^\omega\rangle, \tag{E4}$$

and

$$\begin{aligned}
\mathcal{F}_{ij}^Q &= \frac{1}{4} \text{Re} \left(\langle 0 |^{\otimes n} \prod_{p=0}^{i-1} U_p^\dagger U_i^\dagger \sigma_i \prod_{p=i+1}^{j-1} U_p^\dagger \sigma_j \prod_{p=0}^{j-1} U_p |0\rangle^{\otimes n} \right. \\
&\quad \left. - \langle 0 |^{\otimes n} \prod_{p=0}^{i-1} U_p^\dagger U_i^\dagger \sigma_i \prod_{p=i+1}^k U_p^\dagger |\psi_t^\omega\rangle \langle \psi_t^\omega | \right. \\
&\quad \left. \prod_{p=j+1}^k U_p \sigma_j U_j(\omega_j) \prod_{p=0}^{j-1} U_p |0\rangle^{\otimes n} \right),
\end{aligned} \tag{E5}$$

where we assume that $i < j$ and simplify the notation with $U_p := U_p(\omega_p)$.

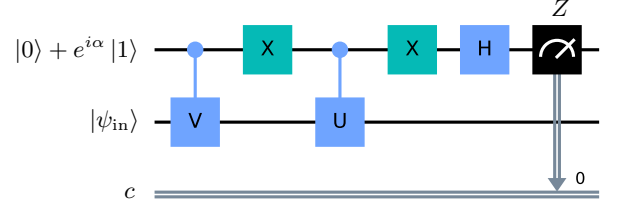


FIG. 8 This quantum circuit – originally proposed in [30] – uses an additional working qubit to evaluate $\text{Re}(e^{i\alpha} \langle \psi_{in} | U^\dagger V | \psi_{in} \rangle)$. Notably, this only requires to measure the working qubit with respect to Z .

One can, now, see that $\text{Im}(C_i - \frac{\partial \langle \psi_t^\omega |}{\partial \omega_i} |\psi_t^\omega\rangle E_t^\omega)$, $\text{Re}(C_i)$ and \mathcal{F}_{ij}^Q may be decomposed into terms of the form $\text{Re}(e^{i\alpha} \langle \psi_{in} | UV | \psi_{in} \rangle)$, respectively $\text{Re}(e^{i\alpha} \langle \psi_{in} | HV | \psi_{in} \rangle)$ using that $\text{Im}(iz) = \text{Re}(z)$. We can, thus, evaluate the equations either with the quantum circuit shown in Fig. 8 or the one presented in Fig. 9.

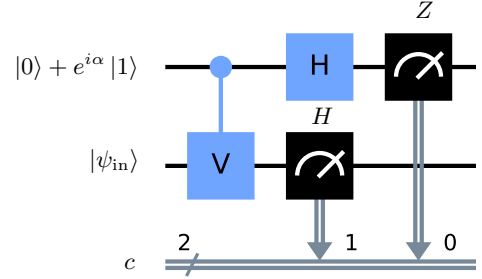


FIG. 9 This quantum circuit uses an additional working qubit to evaluate $\text{Re}(e^{i\alpha} \langle \psi_{in} | HV | \psi_{in} \rangle)$, where the working qubit is measured with respect to Z and the state $|\psi_{in}\rangle$ with respect to the observable H .

Consider, for example, $|\psi_t^\omega\rangle = e^{-i\frac{\omega_1}{2} X} e^{-i\frac{\omega_0}{2} Y} |0\rangle$. Then,

$$\frac{\partial \langle \psi_t^\omega |}{\partial \omega_1} |\psi_t^\omega\rangle = \frac{i}{2} \langle \psi_t^\omega | X | \psi_t^\omega \rangle. \tag{E6}$$

and

$$C_1 = -\frac{i}{2} \langle \psi_t^\omega | H X | \psi_t^\omega \rangle. \tag{E7}$$

To evaluate $\text{Im}(\frac{\partial \langle \psi_t^\omega |}{\partial \omega_1} |\psi_t^\omega\rangle)$ with the circuit shown in Fig. 8, we set $\alpha = -\pi$, $|\psi_{in}\rangle = |\psi_t^\omega\rangle$, $V = X$ and $U = \mathbb{1}$. Furthermore, $\text{Im}(C_1)$, respectively $\text{Re}(C_1)$ can be computed using Fig. 9 with $\alpha = 0$, respectively $\alpha = -\pi/2$,

$|\psi_{\text{in}}\rangle = |\psi_t^\omega\rangle$ and $V = X$. Similarly, the evaluation of

$$\begin{aligned} \mathcal{F}_{01}^Q &= \frac{1}{4} \text{Re} \left(\langle 0 | e^{i\frac{\omega_0}{2}Y} Y X e^{-i\frac{\omega_0}{2}Y} | 0 \rangle \right. \\ &\quad \left. - \langle 0 | Y | 0 \rangle \langle 0 | e^{i\frac{\omega_0}{2}Y} X e^{-i\frac{\omega_0}{2}Y} | 0 \rangle \right) \\ &= \text{Re} \left(\langle 0 | e^{i\frac{\omega_0}{2}Y} Y X e^{-i\frac{\omega_0}{2}Y} | 0 \rangle \right). \end{aligned} \quad (\text{E8})$$

may be conducted with the setup illustrated in Fig. 8 using $\alpha = 0$, $|\psi_{\text{in}}\rangle = e^{-i\frac{\omega_0}{2}Y} | 0 \rangle$, $V = X$ and $U = Y$.

-
- [1] S. Barison, F. Vicentini, and G. Carleo. An efficient quantum algorithm for the time evolution of parameterized circuits. *arXiv preprint - arXiv:2101.04579*, 2021.
- [2] C. Zoufal, A. Lucchi, and S. Woerner. Variational quantum Boltzmann machines. *Quantum Machine Intelligence*, 3(1):7, 2021.
- [3] M. Motta et al. Determining eigenstates and thermal states on a quantum computer using quantum imaginary time evolution. *Nature Physics*, 16(2), 2020.
- [4] K. Temme, T. J. Osborne, K. G. H. Vollbrecht, D. Poulin, and F. Verstraete. Quantum Metropolis sampling. *Nature*, 471, 2011.
- [5] M.-H. Yung and A. Aspuru-Guzik. A quantum–quantum Metropolis algorithm. *Proceedings of the National Academy of Sciences*, 109(3), 2012.
- [6] A. Chowdhury, G. H. Low, and N. Wiebe. A variational quantum algorithm for preparing quantum Gibbs states. *arXiv:2002.00055*, 2020.
- [7] J. Gacon, C. Zoufal, G. Carleo, and S. Woerner. Simultaneous perturbation stochastic approximation of the quantum Fisher information. *arXiv:2103.09232*, 2021.
- [8] S. Lloyd. Universal quantum simulators. *Science*, 273(5278), 1996.
- [9] S. McArdle, T. Jones, S. Endo, Y. Li, S. C. Benjamin, and X. Yuan. Variational ansatz-based quantum simulation of imaginary time evolution. *npj Quantum Information*, 5(1), 2019.
- [10] X. Yuan, S. Endo, Q. Zhao, Y. Li, and S. C. Benjamin. Theory of variational quantum simulation. *Quantum*, 3, 191, 2019.
- [11] R. Martinazzo and I. Burghardt. Local-in-Time Error in Variational Quantum Dynamics. *Phys. Rev. Lett.*, 124, 2020.
- [12] R. Barends et al. Digital quantum simulation of fermionic models with a superconducting circuit. *Nature Communications*, 6(1), 2015.
- [13] J. Gonzalez-Conde, A. Rodriguez-Rozas, E. Solano, and M. Sanz. Pricing financial derivatives with exponential quantum speedup. *arXiv:2101.04023*, 2021.
- [14] F. Fontanela, A. Jacquier, and M. Oumgari. A quantum algorithm for linear PDEs arising in finance. *arXiv:1912.02753*, 2021.
- [15] K. Kubo, Y. O. Nakagawa, S. Endo, and S. Nagayama. Variational quantum simulations of stochastic differential equations. *Physical Review A*, 103(5), 2021.
- [16] S. Endo, J. Sun, Y. Li, S. C. Benjamin, and X. Yuan. Variational quantum simulation of general processes. *Phys. Rev. Lett.*, 125, 2020.
- [17] A. McLachlan. A variational solution of the time-dependent Schrödinger equation. *Molecular Physics*, 8(1), 1964.
- [18] R. Tahir-Kheli. *Ordinary Differential Equations: Mathematical Tools for Physicists*. Springer International Publishing, Cham, 2018.
- [19] S. L. Braunstein and C. M. Caves. Statistical distance and the geometry of quantum states. *Phys. Rev. Lett.*, 72, 1994.
- [20] J. J. Meyer. Fisher information in noisy intermediate-scale quantum applications. *arXiv preprint - arXiv:2103.15191*, 2021.
- [21] J. Liesen and V. Mehrmann. *Linear Algebra*, chapter Linear Systems of Equations. Springer International Publishing, Cham, 2015.
- [22] M. A. Nielsen and I. L. Chuang. *Quantum Computation and Quantum Information*. Cambridge University Press, 2010.
- [23] M. Hayashi. *Quantum Information: An Introduction*. Springer Berlin Heidelberg, Berlin, Heidelberg, 2006.
- [24] D. F. Griffiths and D. J. Higham. *Numerical Methods for Ordinary Differential Equations: Initial Value Problems*, chapter Euler’s Method. Springer London, London, 2010.
- [25] P. Virtanen et al. SciPy 1.0: Fundamental algorithms for scientific computing in python. *Nature Methods*, 17, 2020.
- [26] D. F. Griffiths and D. J. Higham. *Numerical Methods for Ordinary Differential Equations: Initial Value Problems*. Springer London, London, 2010.
- [27] H. Abraham et al. Qiskit: An open-source framework for quantum computing, 2019.
- [28] P. Calabrese, F. H. L. Essler, and M. Fagotti. Quantum quench in the transverse field Ising chain: I. time evolution of order parameter correlators. *Journal of Statistical Mechanics: Theory and Experiment*, 2012.
- [29] C. R. Harris et al. Array programming with NumPy. *Nature*, 585(7825), 2020.
- [30] R. Somma, G. Ortiz, J. E. Gubernatis, E. Knill, and R. Laflamme. Simulating physical phenomena by quantum networks. *Phys. Rev. A*, 65, 2002.